

## Study of ionizing radiation attenuation of glass as: gamma rays shielding material

A. M. Alqahtani<sup>a</sup>, M. S. Alqahtani<sup>b,c</sup>, K. I. Hussein<sup>b,d,\*</sup>, A. J. Alkilib<sup>b</sup>,  
F. F. Alqahtani<sup>e</sup>, N. Elkhoshkhany<sup>f</sup>, I. S. Yaha<sup>g,h</sup>, M. Reben<sup>i</sup>, E. Yousef<sup>g,h</sup>

<sup>a</sup>Medical and Clinical Affairs Department, King Faisal Medical City, Abha 62523, Saudi Arabia

<sup>b</sup>Department of Radiological Sciences, College of Applied Medical Sciences, King Khalid University, Abha 61421, Saudi Arabia

<sup>c</sup>BioImaging Unit, Space Research Centre, Department of Physics and Astronomy, University of Leicester, Leicester LE1 7RH, UK

<sup>d</sup>Department of Medical Physics and Instrumentation, National Cancer Institute, University of Gezira, Wad Medani 20, Sudan.

<sup>e</sup>Department of Radiological Sciences, College of Applied Medical Sciences, Najran University, Najran 1988, Saudi Arabia

<sup>f</sup>Physics Dept., College of Arts and Sciences at Tabrjal, Jouf University, Al-Jouf, Saudi Arabia

<sup>g</sup>Physics Department, Faculty of Science, King Khalid University, Postcode: 9004, Zip code: 61413, Abha, Saudi Arabia

<sup>h</sup>Research Center for Advanced Materials Science (RCAMS), King Khalid University, Postcode: 9004, Zip code: 61413, Abha, Saudi Arabia

<sup>i</sup>Faculty of Materials Science and Ceramics, AGH – University of Science and Technology, al. Mickiewicza 30, 30-059 Cracow, Poland

The primary application of radiation shielding is to safeguard against the harmful effects of radiation. This study investigated the addition of thulium oxide ( $\text{Tm}_2\text{O}_3$ ) to a glass system with a composition of  $75 \text{ TeO}_2\text{--}5 \text{ Li}_2\text{O--}10 \text{ ZnO--}(10\text{-}x)\text{Nb}_2\text{O}_5$ . Multiple radiation-shielding parameters, including linear and mass attenuation coefficients, half-value layers, mean free paths, atomic and electronic cross-sections, effective atomic numbers, and effective electron density, were evaluated. The study compared the half-value layer values of the new composite to those of well-known radiation-shielding materials, which include ordinary concrete and commercial glass. The addition of  $\text{Tm}_2\text{O}_3$  to glass systems efficiently increases the atomic and electronic cross-sections. While all samples had the greatest linear and attenuation coefficients of  $201.5\text{--}232.84 \text{ cm}^2/\text{g}$  at 15 keV, the denser glass had the highest mass attenuation coefficient of  $42.80 \text{ cm}^2/\text{g}$ . The shielding effectiveness depends on the phases structure of  $\text{TeO}_2$  occurred in the prepared glasses.

(Received December 23, 2021; Accepted April 1, 2022)

**Keywords:** Structural of  $\text{TeO}_2$  glass, Density, Mass attenuation coefficient, Half value layer, Radiation shielding

### 1. Introduction

Radiation plays an essential role in many industries such as nuclear research centres, electricity generation, agriculture, and food production (1). High and low levels of radiation doses are used in the diagnosis and treatment of medical cases; these doses can be applied by natural or artificial sources (2,3). Exposing human soft tissues to unwanted radiation or long-term occupational exposure to radiation causes harm to some metabolites and has a genetic effect on DNA, proteins, and lipids, which sometimes results in cancer and death (4,5). To address this issue, radiation shielding is used to reduce the doses received by soft tissues (6). The most utilised

---

\* Corresponding author: kirahim@kku.edu.sa  
<https://doi.org/10.15251/CL.2022.194.227>

radiation shield in nuclear reactors is concrete because of its strength, adaptable design, low price, and its ability to attenuate gamma-rays (7). However, exposing concrete to gamma-rays for prolonged periods leads to fractures and with high radiation energies the water in concrete can evaporate, which affects the protection efficiency of the concrete (8). In addition, concrete is ineffective in the transparency of visible light.







Lead is commonly used in shielding materials due to its reliability. The major environmental disadvantage of lead is its high toxicity; lead is also heavy and expensive (9). Free lead metal powders have been investigated for use as radiation shields by measuring specific parameters such as their thermal and physical characteristics, cost, and radiation protection efficiency (10–12). The improved functionality of glass materials relative to other shielding materials has increased their attractiveness. Glasses based on metal oxide have high attenuation and better optical transparency (13). Additional features that make glass a more appropriate fit for radiation shielding applications are its thermal properties, robust mechanical properties, as well as the ability to change the composition of glass to maintain the required levels of safety (14). They also have numerous desirable environmental and physical properties (15,16). Recycled glass exhibits no changes in its quality and transparency; this decreases the amount of wasted glass and has positive effects on the environment (17). The physical properties of glass include low photo-energies, erosion resistance, high transmission of wavelength and refractive indices, as well as conductivity of electricity (18). Glass is commonly used in the applications of optics such as lasers, fibre optic cables, and solar cells (19,20).

Tellurium dioxide ( $\text{TeO}_2$ ) can expand the applications of glass because of its high mass density and its greater ability to block photons. Various studies show that  $\text{TeO}_2$ -based glass systems have promising applications in radiation protection and optical applications (21). Other study showed that  $\text{TeO}_2$ -glass systems melted together with heavy metal oxides exhibited improved attenuation capabilities compared to lead-based glass systems (22). Furthermore,  $\text{TeO}_2$  demonstrated excellent optical properties (21). investigated  $\text{TeO}_2$ -based glass systems and showed that the glass system cloud utilized for optical applications exhibited  $B_r$  values of more than 0.5 and high radiation emissions during transitions (23). This study uses two pieces of simulation software, MIKE (1) and Py-MLBUF (20, to evaluate and compare the radiation shielding parameters of a glass system with the following composition: 75  $\text{TeO}_2$ –5  $\text{Li}_2\text{O}$ –10  $\text{ZnO}$ –(10- $x$ )  $\text{Nb}_2\text{O}_5$ – $x$   $\text{Tm}_2\text{O}_3$ .

## 2. Materials and methods

Several compositions of the tellurite glass system were prepared (22); they had the composition 75  $\text{TeO}_2$ –5  $\text{Li}_2\text{O}$ –10  $\text{ZnO}$ –(10- $x$ )  $\text{Nb}_2\text{O}_5$ – $x$   $\text{Tm}_2\text{O}_3$ , where  $x$  was 0, 0.5, 1.0, 1.5, 2.0, 2.5 mol%. The samples were labelled TLZNT1, TLZNT2, TLZNT3, TLZNT4, TLZNT5, and TLZNT6, respectively, and are listed in Table 1. The glass systems were investigated under a range of photon energies through the use of two pieces of simulation software. The Py-MLBUF software investigates the radiation shielding properties of glass over a range of photon energies, while the MIKE software investigates the behaviour of the glass system over a range of photon energies, focusing on its optical parameters and its radiation shielding applications.

Table 1. The composition wights and densities of TLZNT glasses (22).

Sample code	Compsation (mol%)					Density (g/cm <sup>3</sup> )	Sample Appearance
	TeO <sub>2</sub>	Li <sub>2</sub> O	ZnO	Nb <sub>2</sub> O <sub>5</sub>	Tm <sub>2</sub> O <sub>3</sub>		
TLZNT1	75	5	10	10	0	5.28	
TLZNT2	75	5	10	9.5	0.5	5.32	
TLZNT3	75	5	10	9	1	5.34	
TLZNT4	75	5	10	8.5	1.5	5.38	
TLZNT5	75	5	10	8	2	5.40	
TLZNT6	75	5	10	7.5	2.5	5.44	

The glass samples were prepped with chemicals with 99.9% purity and melted by using traditional quenching techniques.

The TLZNT glasses samples were simulated over a range of photon energies from 15 keV–20 MeV. The LAC was first measured using the Beer-Lambert Law, also known as the exponential beam attenuation law(24). The equation of LAC can be described as follows:

$$I = I_0 e^{-\mu x} \quad (1)$$

The mathematical equation described above expresses the relationship between the attenuated ionizing photons ( $I$ ) and the unattenuated ionizing photons ( $I_0$ ) which pass through a specific thickness of the simulated material ( $x$ ). In addition,  $\mu$  describes the LAC which is related to the density and photo-energy function of the sample. Greater values of  $\mu$  indicate that the material blocks more photons.

MAC is the main shielding parameter measured by both software packages. It describes the material's ability to attenuate incident photons energies and is calculated as follows:

$$MAC = \frac{\mu}{\rho} = \sum_i W_i \left( \frac{\mu}{\rho} \right)_i \quad (2)$$

The LAC material density and photo-energy function of the samples are represented by  $\mu$ ,  $\rho$ ,  $W_i$  and  $\left( \frac{\mu}{\rho} \right)_i$ , respectively, where ith constituent elements of MAC.

Another shielding factor, HVL, can be used to determine the thickness of the glass samples. It can also be used to decrease the incident photons energies intensity to half its initial value and is calculated as follows:

$$HV = \frac{\ln(2)}{LAC} \quad (3)$$

The MPF is a significant factor that describes the shielding ability of the glass samples against photons energies. It is described as the mean distance travelled by the high photon energies between two sequential interactions and is calculated as follows:

$$MP = 1/\mu \quad (4)$$

$Z_{\text{eff}}$  is another parameter used to evaluate the radiation shielding properties of multi-element glasses samples. It can be differentiated with a pure sample as to atomic number. The values of  $Z_{\text{eff}}$  in this study were mathematically calculated as follows:

$$Z_{\text{eff}} = \frac{\sum_i f_i A_i \left(\frac{\mu}{\rho}\right)_i}{\sum_j \frac{A_j}{Z_j} \left(\frac{\mu}{\rho}\right)_j} \quad (5)$$

where  $A$  represents the atomic mass per mole,  $f$  is the molar fraction, and  $Z$  is the atomic number of the component element.

Table 2 A. MAC relative deviations (RD) for TLZNT1, TLZNT2 and TLZNT3 glasses by using MIKE and Py-MLBUF.

Photon energy	TLZNT1			TLZNT2			TLZNT3		
(MeV)	MIKE	Py-MLBUF	RD%	MIKE	Py-MLBUF	RD%	MIKE	Py-MLBUF	RD%
0.5	0.09	0.09	0.33	0.09	0.09	0.58	0.09	0.09	0.83
0.6	0.08	0.08	0.10	0.08	0.08	0.28	0.08	0.08	0.46
0.8	0.07	0.07	-0.13	0.07	0.07	-0.03	0.07	0.07	0.06
1	0.06	0.06	-0.25	0.06	0.06	-0.19	0.06	0.06	-0.13
1.5	0.05	0.05	-0.31	0.05	0.05	-0.29	0.05	0.05	-0.26
2	0.04	0.04	-0.21	0.04	0.04	-0.17	0.04	0.04	-0.14
2.5	0.04	0.04	-0.03	0.04	0.04	0.02	0.04	0.04	0.07
3	0.04	0.04	0.15	0.04	0.04	0.22	0.04	0.04	0.28
4	0.03	0.03	0.52	0.03	0.03	0.62	0.03	0.03	0.71
5	0.03	0.03	0.84	0.03	0.03	0.96	0.03	0.03	1.09
6	0.03	0.03	1.10	0.03	0.03	1.25	0.03	0.03	1.40
8	0.03	0.03	1.52	0.03	0.03	1.70	0.03	0.03	1.88

Table. 2 B. MAC relative deviations (RD) for TLZNT4, TLZNT5 and TLZNT6 glasses by using MIKE and Py-MLBUF.

Photon energy	TLZNT4			TLZNT5			TLZNT6		
(MeV)	MIKE	Py-MLBUF	RD%	MIKE	Py-MLBUF	RD%	MIKE	Py-MLBUF	RD%
0.5	0.09	0.09	1.07	0.09	0.09	1.30	0.09	0.09	1.49
0.6	0.08	0.08	0.63	0.08	0.08	0.75	0.08	0.08	0.92
0.8	0.07	0.07	0.16	0.07	0.07	0.26	0.07	0.07	0.41
1	0.06	0.06	-0.07	0.06	0.06	-0.01	0.06	0.06	0.08
1.5	0.05	0.05	-0.24	0.05	0.05	-0.19	0.05	0.05	-0.16
2	0.04	0.04	-0.11	0.04	0.04	-0.11	0.04	0.04	-0.07
2.5	0.04	0.04	0.11	0.04	0.04	0.08	0.04	0.04	0.15
3	0.04	0.04	0.34	0.04	0.04	0.47	0.04	0.04	0.57
4	0.03	0.03	0.81	0.03	0.03	0.89	0.03	0.03	1.05
5	0.03	0.03	1.21	0.03	0.03	1.20	0.03	0.03	1.41
6	0.03	0.03	1.54	0.03	0.03	1.73	0.03	0.03	1.68
8	0.03	0.03	2.06	0.03	0.03	2.12	0.03	0.03	2.43

The  $N_{\text{eff}}$  factor has a significant contribution to the material's shielding properties. It represents the electron density and is calculated as follows:

$$N_{\text{eff}} = \frac{N_A Z_{\text{eff}}}{\langle A \rangle} \quad (6)$$

where  $\langle A \rangle = \sum_i f_i A_i$  is the average atomic mass of the glass samples. Two more factors that are used to measure the interaction between photons energies and the atoms and electrons of the samples are the ACS and ECS, respectively. They are mathematically expressed using the equations below:

$$ACS = \sigma_e = \frac{\sum_n f_n A_n}{N_A} \mu_m \quad (7)$$

$$ECS = \sigma_e = \left[ \frac{1}{N_A} \right] = \sum_i i \left[ \frac{f_i A_i}{Z_i} (\mu_m)_i \right] \quad (8)$$

where  $Z_i$  represents the atomic number,  $N_A$  is Avogadro's number, and  $A_i$  is the atomic weight of the  $i$ -th element in grams.

Recently, several simulation software packages have used Monte Carlo (MC) techniques to study radiation shielding. This technique has numerous advantages, including geometry construction pliability, scalability of energy, and defined innumerable scorers (25). The MIKE simulation software was coded in MATLAB and used to calculate and analyze different shielding parameters, such as LAC, MAC, HVL, MFP,  $Z_{\text{eff}}$ ,  $N_{\text{eff}}$ ,  $C_{\text{eff}}$ , R, and TF. This software is also able to measure the physical properties of the whole mixture and the elements of compound materials, as well as its shielding parameters. The atomic number of elements used to calculate the MAC energy parameter was imported from the NIST WinXcom database for energy levels between 1 keV–100 MeV (26). Moreover, MIKE can provide different physical properties and shielding parameters at user-selected energies for standard and commercial materials such as RS 253, RS 360, RS 520 G18, barite, chromite, ferrite, and magnetite (26).

### 3. Results

The parameters of the six TLZNT glass samples were estimated using MIKE and Py-MLBUF. The values of the MAC parameter were obtained from both pieces of software between 500 keV–8 MeV; the differences between the results are compared in Table 2.A and 2.B.

As shown in Table 2.A and 2.B, the theoretical MAC value of all six TLZNT glass samples was calculated to be higher in MIKE than in Py-MLBUF. The relative deviations (RD) between the results of the two pieces of software were measured using the formula below:

$$RD(\%) = 100 \times \frac{MAC_{MIKE} - MAC_{Py-MLBUF}}{MAC_{MIKE}} \quad (9)$$

Overall, the RD percentage was measured between the energy ranges of 600 keV to 4 MeV. The lowest percentages were recorded at the 1.5 MeV energy levels; TLZNT1, TLZNT2, TLZNT3, TLZNT4, TLZNT5, and TLZNT6 had RD percentages of -0.31%, -0.28%, -0.26%, -0.23%, -0.19%, and -0.16%, respectively. In contrast, the highest percentages were recorded at 4 MeV; TLZNT1, TLZNT2, TLZNT3, TLZNT4, TLZNT5, and TLZNT6 exhibited RD percentages of 0.51%, 0.61%, 0.71%, 0.80%, 0.88%, and 1.04%, respectively.

The difference between simulated and theoretically calculated MAC values between the energy range of 500 keV–8 MeV are shown Table2. The figures shows that the discrepancies between the MIKE and Py-MLBUF results are lower at medium and high energies. In addition, it was observed that the bulk of the MAC values computed by MIKE were higher than those found by the Py-MLBUF simulation. The theoretical variation of MAC values against photon energies in the 15 keV–15 MeV range obtained by MIKE are shown in Figure 1. The MAC values are shown to progressively rise from TLZNT1 to TLZNT6. For example, at 15 keV, the MAC values of TLZNT1–TLZNT6 increase from 38.1 to 41.3 cm<sup>2</sup>/g. It was also observed that the greatest MAC values occurred at the lower energies while the lowest MAC values occurred at the higher energies for all glass samples.

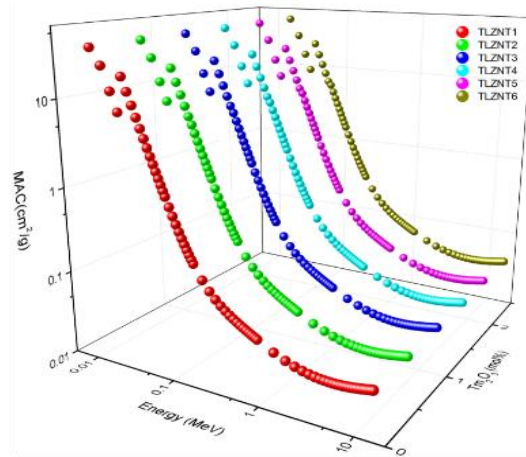


Fig. 1. The 3D: line graph of MAC for all TLZNT glass.

### 4. Discussion

Figure 1 shows that the MAC values evaluated by MIKE drop sharply as photon energy increases, which may be attributed to the dominance of the photoelectric effect at low energies, as the cross-section of photoelectric absorption (PEA) approximately changes with  $E^{-3.5}$  (16). Compton scattering (CS) becomes prominent in the intermediate photon energy range, and the cross-section varies with  $E$  and  $Z$ . However, beyond 4 MeV, a small rise in the MAC values of the glasses was observed. This rise is the result of the interaction between CS and pair production

(PP) processes. Additionally, a sharp rise in the  $\text{Tm}_2\text{O}_3$  in the composition of the glass systems from  $5.28 \text{ g/cm}^3$  to  $5.44 \text{ g/cm}^3$  is observed around 15 keV for TLZNT1–TLZNT6. Due to the absence of  $\text{Tm}_2\text{O}_3$  in TLZNT1, this abrupt rise was not seen in this sample.

This implies that TLZNT glasses are promising materials for use as protective shields against ionizing radiation, such as gamma rays. Furthermore, Figure 2 presents the LAC values, which are calculated as a function of photon energy by combining the calculated mass attenuation coefficients with the measured sample densities. The computed LAC values increased with increasing density. The addition of  $\text{Tm}_2\text{O}_3$  raised the density of samples TLZNT1 through TLZNT6, with a constant density of TLZNT. Therefore, TLZNT1 had the lowest LAC value while the TLZNT6 sample had the highest LAC value due to it possessing the highest density. It is worth noting that the attenuation capacities of samples are strongly influenced by the incident photon energy. For example, the LAC values of TLZNT4 were reduced from 108.85 to  $77 \text{ cm}^{-1}$  between 0.035–0.04 MeV, a difference of 34.27%. In contrast, larger energies resulted in lower LAC values of 0.188 and  $0.178 \text{ cm}^{-1}$ , respectively (5.46% difference) between 3.5–5.5 MeV.

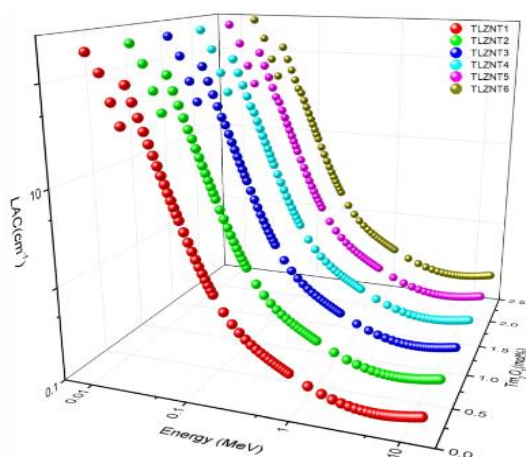


Fig. 2 3D. The 3D line graph of LAC for all TLZNT glass.

The ECS and ACS values of all samples were analyzed over the same range of energies. Materials with greater ECS and ACS values will absorb and attenuate incident radiation more effectively. The effect of additional  $\text{Tm}_2\text{O}_3$  content in TLZNT on both the ECS and ACS was studied. The variation in the simulated ECS and ACS values with different incident photon energies were calculated using Equations 7 and 8 and are shown in Figures 3A and 3B. TLZNT samples doped with  $\text{Tm}_2\text{O}_3$  exhibit increased ACS values of approximately  $3.47536 \times 10^{-21} \text{ cm}^2/\text{g}$  (Figure 3a), which abruptly decreases at energy 15 keV. This is due to the photoelectric mode of absorption at low photon energy, where the probability of CS is minimal. Figure 3A illustrates the dependency of ECS on photon energy for each sample. The insert at the top of the graph shows that TLZNT6, which has the greatest density, exhibited significantly improved ECS values even at high energy photons. This is because the sample's higher electron density increases the likelihood of photons interacting through CS and pair formation.

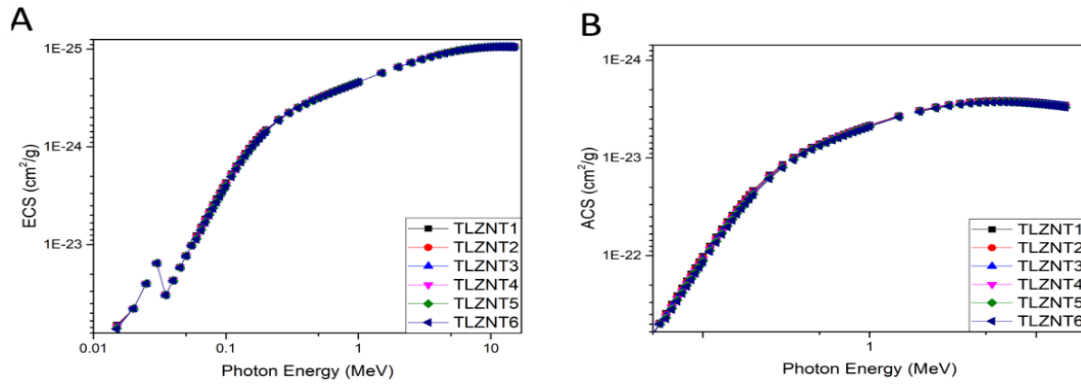


Fig. 3. A and B: line graph of ECS and ACS for all TLZNT glass.

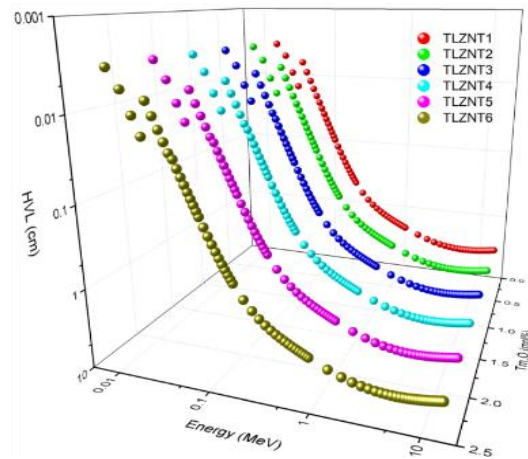


Fig. 4 3D: line graph of HVL for TLZNT glasses.

Figure 4 depicts the change in the HVL values of TLZNT glasses when exposed to various photon energies. It demonstrates that TLZNT6 glass had the lowest HVL values ranging from 0.0029–3.4 cm and that TLZNT1 glass had the greatest HVL values ranging from 0.0034–3.58 cm. This suggests that an increase in the  $\text{TiO}_2$  ratio in the samples results in a reduction in HVL values, which in turn increases the shielding effectiveness of the glass samples. All TLZNT glasses exhibit the lowest HVL values at lower photon energies (Fig. 4), and this behaviour may be explained by the dominance of the photoelectric effect at this energy level. A steady rise in HVL values was observed as the energy increased from 0.3–5 MeV. This is due to the predominance of CS in this region of the spectrum of light. Finally, the small rise in HVL values at higher energies after 5 MeV is likely due to pair formation.

Figure 5 illustrates the variation in MFP values of the studied glasses as a function of photon energy in the 0.015 keV–15 MeV energy range. MFP values have a similar dependency on photon energy as HVL values; this suggests that the same arguments about photon interactions apply to MFP values as well. As the energy level increased, the MFP values dropped from TLZNT1 to TLZNT6, which suggests that a photon in this energy range can penetrate through TLZNT1 more effectively compared to the other glass samples.



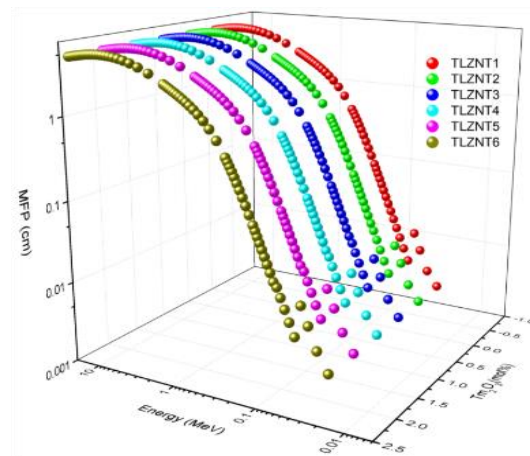


Fig. 5 3D: line graph of MPF for all TLZNT glass.

The HVL values of the TLZNT glasses were also other commercial materials in the literature, such as RS 253, RS 360, RS 520 G18, barite, chromite, ferrite, and magnetite. TLZNT6 was observed to be a promising material for shielding against gamma rays in this energy range (Figs. 6).

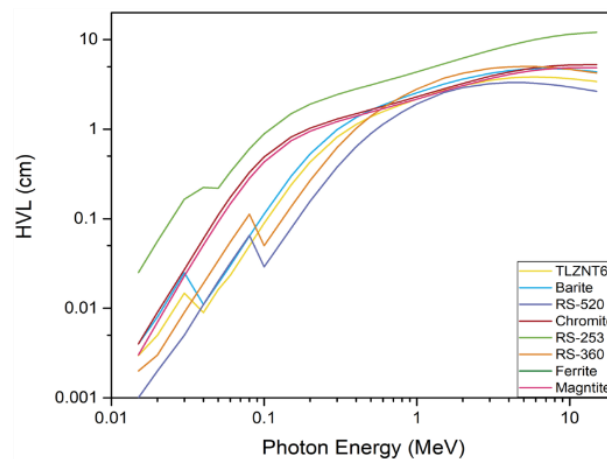


Fig. 6. The line graph shows the HVL of TLZNT compare to other well-known stander glasses.

The  $Z_{\text{eff}}$  and  $N_{\text{eff}}$  values for each TLZNT sample were calculated using Equations 5 and 6. The MIKE 15 keV–15 MeV Photon Cross-Sectional Library was utilized in this phase of the research. Figures 7 and 8 illustrate the variation of  $Z_{\text{eff}}$  and  $N_{\text{eff}}$  with photon energy, respectively. These figures, which follow from Hine's proposal, demonstrate that both parameters are functions that are highly reliant on the incident photon energy (17). This was expected because the mass attenuation coefficients ( $Z_{\text{eff}}$ ) for all photons of any energy level (Eq. 5) are dependent on the mass attenuation coefficients of the different component elements (thus the total photon cross-section) (Eq. 6). Both  $Z_{\text{eff}}$  and  $N_{\text{eff}}$  appear to be nearly entirely dependent on photon energy and have similar dependency patterns (Figs. 7 and 8).

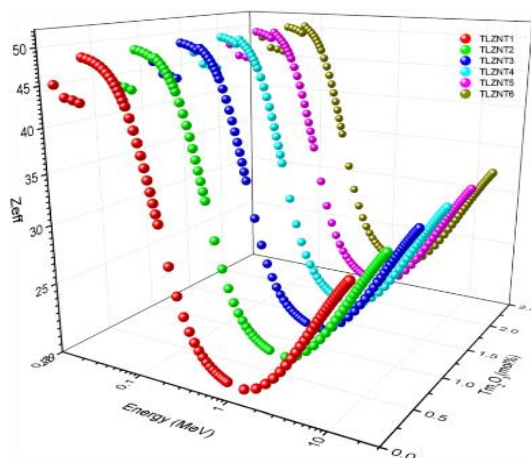


Fig. 7 3D: line graph shows  $Z_{\text{eff}}$  for all TLZNT glass.

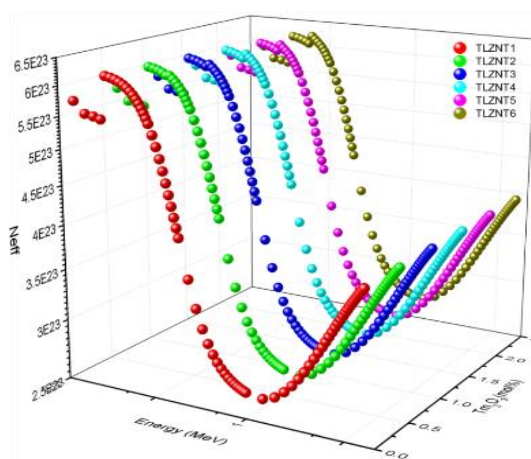


Fig. 8 3D: line graph shows  $N_{\text{eff}}$  for all TLZNT glass.

This section addresses the importance of basic PP interactions in conjunction with mass attenuation coefficients. It is possible to classify these photon interactions depending on their dominance, and they are separated into four distinct groups: photoelectric absorption in the low energy region, CS in the medium energy region, the partial photon in the region of the nucleus, and CS in the high energy region. Due to the insignificant role of coherent scattering and pair formation in the context of the electron, the influence of Rayleigh (coherent) scattering and pair generation is almost unnoticeable. Rayleigh scattering occurs when photoelectric processes predominate; therefore, it occurs at low photon energies. In contrast, in the area of the nuclei, there is a large variation in pair creation at  $Z^2$ , while electron pair production only changes by  $Z$  (18). The highest values of  $Z_{\text{eff}}$  were achieved in the low energy zone for all samples (Fig. 7). TLZNT1–TLZNT6 had the following values: 45.35, 45.88, 46.39, 46.89, 47.38, and 47.84, respectively. The variance in the lower energy area for the  $Z_{\text{eff}}$  curves was similar in all TLZNT glass systems, with the exception of TLZNT1. TLZNT1 glass system is missing  $\text{Tm}_2\text{O}_3$ , which is found in TLZNT1 which has  $\text{Tm}_2\text{O}_3$ . The abrupt increases in the curves of TLZNT1–TLZNT6 that occur immediately after 15 keV may also be explained by the presence of Zr in the structure of each glass system. Atomic K-shell absorption of  $\text{Tm}_2\text{O}_3$  results in the absorption observed at 0.018 MeV. The highest magnitude for TLZNT6 is due to the quantity of  $\text{Tm}_2\text{O}_3$  in the sample, while the smallest magnitude for TLZNT1 is due to the absence of  $\text{Tm}_2\text{O}_3$  in the sample. This assessment suggests that glass may contribute significantly to  $Z_{\text{eff}}$ , and that  $\text{Tm}_2\text{O}_3$  concentrations have a beneficial impact at low energies where photoelectric absorption is prominent. After the rapid drop

in photon energy, the photoelectric effect on  $Z_{\text{eff}}$  disappears and CS becomes the dominant interaction type. The steep inclination of the transition zone is due to the combined contributions of photoelectric and Compton interactions. The lowest values of  $Z_{\text{eff}}$  are found in this intermediate energy range (Fig. 7). TLZNT1–TLZNT6 are found to have values of 30.48, 30.73, 30.99, 31.25, 31.51, and 31.76 for each of the values, respectively. Compton area glass systems have had their effective atomic numbers calculated.

The  $Z_{\text{eff}}$  values of each glass system stay fairly constant between 0.3–5 MeV. This shows that the chemical composition of the TLZNT glasses becomes less significant when the Compton interaction is dominant. Pair formation (in the nucleus field) dominates between 5–15 MeV (Fig. 7). The combined impact of the Compton and pair formation interactions may be attributed to the modest increase in the  $Z_{\text{eff}}$  curve as a function of photon energy. As Z2 affects pair formation, it is important to consider the chemical composition of the glass systems. Hence, the  $Z_{\text{eff}}$  values in this final area begin to be higher than those in the Compton region. This explains why  $Z_{\text{eff}}$  values decrease from TLZNT6 to TLZNT1.

Figure 8 illustrates the photon energy dependence of effective electron densities ( $N_{\text{eff}}$ ) in each TLZNT glass system. There is a strong relationship between  $N_{\text{eff}}$  and  $Z_{\text{eff}}$  (Eq. 6). A qualitative analysis of this figure shows that the variation of  $N_{\text{eff}}$  as a function of photon energy may be explained in the same manner that the variation of  $Z_{\text{eff}}$  was explained (Fig. 7). Thus, the differences in  $N_{\text{eff}}$  values across the energy spectrum can be explained by the major photon interactions with glass materials and the chemical composition of the glass systems. However, the most striking feature of Figure 7 is the near proximity of  $N_{\text{eff}}$  values between 0.3–5 MeV. As previously mentioned, the  $Z_{\text{eff}}$  values of the TLZNT glasses are almost identical to the mean atomic numbers,  $\langle Z \rangle$ s. Consequently, the effective electron densities of each glass are almost identical. This is illustrated by the dark dashed line in Figure 7. This suggests that the gamma-ray shielding ability of the TLZNT glasses in the intermediate energy range is less dependent on their chemical composition. The  $N_{\text{eff}}$  values of the TLZNT glass samples are inversely related to their average atomic weight. Since the change in  $Z_{\text{eff}}$  is greater than the change in atomic weight, the  $N_{\text{eff}}$  values increase as the  $\text{Tm}_2\text{O}_3$  ratio increases.

#### 4. Conclusions

This study investigated the shielding properties of  $\text{Tm}_2\text{O}_3$ . The glass system 75  $\text{TeO}_2$ –5  $\text{Li}_2\text{O}$ –10  $\text{ZnO}$ –(10– $x$ )  $\text{Nb}_2\text{O}_5$ – $x$   $\text{Tm}_2\text{O}_3$  was investigated where  $x$  was equal to 0, 0.5, 1.0, 1.5, 2.0, and 2.5 mol%. The mass attenuation coefficients for six distinct TLZNT glass systems were simulated using MIKE for photon energies within the 0.015–15 MeV range. Small relative differences were obtained with the Py-MLBUF simulation program. The  $Z_{\text{eff}}$  and  $N_{\text{eff}}$  values of the TLZNT glasses were strongly dependent on the energy of the incident photon. The presence of  $\text{Tm}_2\text{O}_3$  in the glass system is found to have a beneficial effect on the magnitudes of  $Z_{\text{eff}}$  and  $N_{\text{eff}}$  across the entire energy range. As the energy levels were increased from 0.3–5 MeV, an increase in the HVL readings was detected. The energy in the moderate energy zone. Compton scattering is present across this part of the spectrum of light. The modest increase in HVL values at approximately 5 MeV can be attributed to the pairing process. MFP values had a similar dependence on photon energy as the HVL values, suggesting that the same arguments about photon interactions apply to MFP values as well.

TLZNT1 is the least efficient at shielding a photon at this energy level. The TLZNT glasses were also compared to other commercial materials in the literature, such as RS 253, RS 360, RS 520 G18, barite, chromite, ferrite, and magnetite. TLZNT6 was found to be a good gamma-ray shielding material in this energy range. In scenarios where heavier elements such as Pb (lead) or Bi (bismuth) cannot be used to enhance the gamma-ray shielding properties of glasses,  $\text{Tm}_2\text{O}_3$  can be used as a suitable alternative. The results indicate that increasing the concentration of  $\text{Tm}_2\text{O}_3$  in TLZNT glasses improves their nuclear shielding properties.

## Acknowledgments

The authors extend their appreciation to the Deanship of Scientific Research at King Khalid University (KKU) for funding this research project Number (R.G.P2/79/41). Furthermore, this work was supported by the Ministry of Education in the Kingdom of Saudi Arabia through project number IFP-KKU-2020/8

## References

- [1] Hussein KI, Alqahtani MS, Algarni H, Zahran H, Yaha IS, Grelowska I, et al. Journal of Instrumentation **16**(07), T07004 (2021); <https://doi.org/10.1088/1748-0221/16/07/T07004>
- [2] Kulwinder Singh Mann, Sukhmanjit Singh Mann, Annals of Nuclear Energy, 107845 (2021).
- [3] Y. S. Rammah, M. S. Al-Buriah, F. I. El-Agawany, Y. M. AbouDeif, E. S. Yousef, Ceram. Int. **46**, 27561 (2020); <https://doi.org/10.1016/j.ceramint.2020.07.248>
- [4] Y. S. Rammah, F. I. El-Agawany, A. M. Abu El Soad, E. Yousef, I. A. El-Mesady, Ceram. Int. **46**, 22766 (2020); <https://doi.org/10.1016/j.ceramint.2020.06.043>
- [5] Y. S. Rammah, I. O. Olarinoye, F. I. El-Agawany, A. El-Adawy, E. S. Yousef, Ceram. Int. **46**, 27163 (2020); <https://doi.org/10.1016/j.ceramint.2020.07.197>
- [6] J. H. Kim, The Korean journal of pain **31**(3), 145 (2018); <https://doi.org/10.3344/kjp.2018.31.3.145>
- [7] A. Azuraida, M. K. Halimah, M. Ishak, N. R. Fadhilah, A. Norhayati, N. Ahmad. Chalcogenide Letters, **18**(3), 123 (2021)
- [8] C.-M. Lee, Y. H. Lee, K. J. Lee, Progress in Nuclear Energy **49**(4), 303 (2007); <https://doi.org/10.1016/j.pnucene.2007.01.006>
- [9] N. Aral, F. B. Nergis, C. Candan, Textile Research Journal **86**(8), 803 (2016); <https://doi.org/10.1177/0040517515590409>
- [10] J. P. McCaffrey, F. Tessier, H. Shen, Medical Physics **1**(39)(7Part1), 4537 (2012); <https://doi.org/10.1118/1.4730504>
- [11] Jamal AbuAlRoos N, Azman MN, Baharul Amin NA, Zainon R., Physica Medica **78**, 48 (2020); <https://doi.org/10.1016/j.ejmp.2020.08.017>
- [12] Li Z, Zhou W, Zhang X, Gao Y, Guo S., Scientific Reports **11**(1), 4384 (2021); <https://doi.org/10.1038/s41598-021-83031-4>
- [13] Mehrara R, Malekie S, Kotahi SMS, Kashian S., Scientific Reports **11**(1), 10614 (2021), <https://doi.org/10.1038/s41598-021-89773-5>
- [14] Alhadeethi Y., Ceramics International **1**, 46 (2020).
- [15] A. Azuraida, M. K. Halimah, M. Ishak, L. Hasnimulyai, S. I. Ahmad, Chalcogenide Letters, **17**(4), 187 (2020).
- [16] Lezal D, Pedlikova J, Kostka P, Bludská J, Poulain M, Zavadil J., Journal of Non-Crystalline Solids **284**(1), 288 (2001); [https://doi.org/10.1016/S0022-3093\(01\)00425-2](https://doi.org/10.1016/S0022-3093(01)00425-2)
- [17] Rabelo Monich P, Lucas H, Friedrich B, Bernardo E., Ceramics **4**, 2021; <https://doi.org/10.3390/ceramics4010001>
- [18] Akyildirim H, Kavaz E, El-Agawany FI, Yousef E, Rammah YS., Journal of Non-Crystalline Solids **545**, 120245 (2020); <https://doi.org/10.1016/j.jnoncrysol.2020.120245>
- [19] MacFarlane DR, Newman PJ., In: ProcSPIE, 1998.
- [20] Basu K, Selopal GS, Mohammadnezad M, Akilimali R, Wang ZM, Zhao H, et al., Electrochimica Acta **349**, 136409 (2020); <https://doi.org/10.1016/j.electacta.2020.136409>
- [21] Elkhoshkhany N, Marzouk SY, Shahin S., Journal of Non-Crystalline Solids **472**, 39 (2017); <https://doi.org/10.1016/j.jnoncrysol.2017.07.012>
- [22] N. Elkhoshkhany, Samir Marzouk, M. El-Sherbiny, Sally Yousri, Mohammed S. Alqahtani, H. Algarni, Manuela Reben, ElSayed Yousef, Results in Physics **24**, 104202 (2021); <https://doi.org/10.1016/j.rinp.2021.104202>

- [23] Rolli R, Gatterer K, Wachtler M, Bettinelli M, Speghini A, Ajò D., *Spectrochimica Acta Part A: Molecular and Biomolecular Spectroscopy* **57**(10), 2009 (2001); [https://doi.org/10.1016/S1386-1425\(01\)00474-7](https://doi.org/10.1016/S1386-1425(01)00474-7)
- [24] Swinehart DF., *Journal of Chemical Education* **39**(7), 333 (1962); <https://doi.org/10.1021/ed039p333>
- [25] Oliveira AD, Oliveira C., *Radiation Protection Dosimetry* **115**(1–4), 254 (2005); <https://doi.org/10.1093/rpd/nci187>
- [26] D.K. Gaikwad, S.S. Obaid, M.I. Sayyed, R.R. Bhosale, V. V. Awasarmol, A. Kumar, M.D. Shirsat, P.P. Pawar, *Mater. Chem. Phys.* **213**, 508 (2018); <https://doi.org/10.1016/j.matchemphys.2018.04.019>
- [27] Hehn G., *Nuclear Technology* **74**(1), 104 (1986); <https://doi.org/10.13182/NT86-A33824>
- [28] Hine GJ, Brownell GL. Note Added in Second Printing. In: Hine GJ, Brownell GLBT-RD, editors. Academic Press; 1956. p. viii; <https://doi.org/10.1016/B978-1-4832-3257-7.50005-6>
- [29] Singh VP, Badiger NM, Kaewkhao J., *Journal of Non-Crystalline Solids* **404**, 167 (2014); <https://doi.org/10.1016/j.jnoncrysol.2014.08.003>